nature structural & molecular biology

Crystal structure of a BRAF kinase domain monomer explains basis for allosteric regulation

Neroshan Thevakumaran[1,2,7], Hugo Lavoie[3,7], David A Critton[4], Andrew Tebben[4], Anne Marinier[3], Frank Sicheri[1,2,5] & Marc Therrien[3,6]

Reported RAF kinase domain structures adopt a side-to-side dimer configuration reflective of an 'on' state that underpins an allosteric mechanism of regulation. Atomic details of the monomer 'off' state have been elusive. Reinspection of the BRAF kinase domain structures revealed that sulfonamide inhibitors induce features of an off state, primarily a laterally displaced helix αC stabilized by the activation segment helix 1 (AS-H1). These features correlated with the ability of sulfonamides to disrupt human BRAF homodimers in cells, *in vitro* and in crystals yielding a structure of BRAF in a monomer state. The crystal structure revealed exaggerated, nonproductive positions of helix αC and AS-H1, the latter of which is the target of potent BRAF oncogenic mutations. Together, this work provides formal proof of an allosteric link between the RAF dimer interface, the activation segment and the catalytic infrastructure.

RAF kinase activity is regulated through adoption of a unique side-to-side dimer configuration of its kinase domain[1] and additionally by a more general mechanism involving phosphorylation on sites within the kinase-domain activation segment (AS)[2,3]. Dimerization is now firmly established as a key step in both the physiological and oncogenic activation of RAF[4–6]. It is also widely accepted as the main contributing cause of paradoxical transactivation of RAF kinase function by many small-molecule kinase inhibitors in experimental and clinical settings[6–8]. BRAF mutations are a major cause of human cancer[9,10], with ~98% of oncogenic alterations mapping to the kinase-domain AS[11]. The most common AS mutations involve substitutions of Val600 with glutamate. Similar in principle to regulation by AS phosphorylation, oncogenic mutations can be inferred to act by promoting a productive on-state conformation and/or by destabilizing a nonproductive off-state conformation of the AS and the surrounding catalytic cleft[5]. Precisely how each BRAF oncogenic mutation acts in this regard has remained an open question because a representative off-state monomer structure to complement the numerous presumptive on-state dimer structures has remained elusive. In addition, in many of the on-state dimer structures, major portions of the AS are disordered, so an accurate reference point of the on state is partly obscured. Last, because all BRAF structures solved to date have been complexed to small-molecule inhibitors, it has been difficult to precisely disentangle which features of kinase-domain structure reflect inhibitor-induced artifacts versus natural aspects of the enzyme's structure and function. With these issues in mind, we sought to reanalyze the large body of RAF structural information available with the hope of uncovering overlooked aspects of the enzyme's structure and regulatory function.

RESULTS

Helix αC distortions correlate with dimer-breaker properties

To discern possible features of the RAF kinase off state, we revisited the large repertoire of 34 RAF structures deposited in the Protein Data Bank and uncovered a subpopulation of ten highly similar outlier structures characterized by lateral movement of helix αC by ~5 Å and the presence of a supporting helix AS-H1 within the kinase AS (**Fig. 1a** and **Supplementary Table 1**), a helix whose functional significance has been largely overlooked. With respect to these outlier features, the ten co-structures more closely resemble an off-state epidermal growth factor receptor (EGFR) kinase structure, whereas the remaining 24 BRAF kinase domain co-structures more closely resemble on-state EGFR kinase structures (**Fig. 1b**)[12]. Furthermore, we noticed paralogous kinase domains with ASs adopting conformations similar to the conformation of helix AS-H1 in a number of other off-state structures (described below)[12–14]. From these structural observations and follow-on biochemical, biophysical and functional analyses, we deduced that this subpopulation of inhibitor-bound structures are largely representative of the physiological off state of BRAF corresponding to the monomer configuration with a dephosphorylated AS.

All ten outlier structures correspond to complexes with a single class of related sulfonamide inhibitors with highly variable planar aromatic substituents in the R_2 position and hydrophobic alkyl (or aryl-1) moieties in the R_1 position (**Supplementary Fig. 1a**).

[1]Lunenfeld-Tanenbaum Research Institute, Mount Sinai Hospital, Toronto, Ontario, Canada. [2]Department of Biochemistry, University of Toronto, Toronto, Ontario, Canada. [3]Institute for Research in Immunology and Cancer, Université de Montréal, Montréal, Québec, Canada. [4]Molecular Structure & Design Group, Molecular Discovery Technologies Department, Bristol-Myers Squibb Research, Princeton, New Jersey, USA. [5]Department of Molecular Genetics, University of Toronto, Toronto, Ontario, Canada. [6]Département de Pathologie et Biologie Cellulaire, Université de Montréal, Montréal, Québec, Canada. [7]These authors contributed equally to this work. Correspondence should be addressed to M.T. (marc.therrien@umontreal.ca) or F.S. (sicheri@lunenfeld.ca).

Received 13 August; accepted 3 November; published online 1 December 2014; doi:10.1038/nsmb.2924

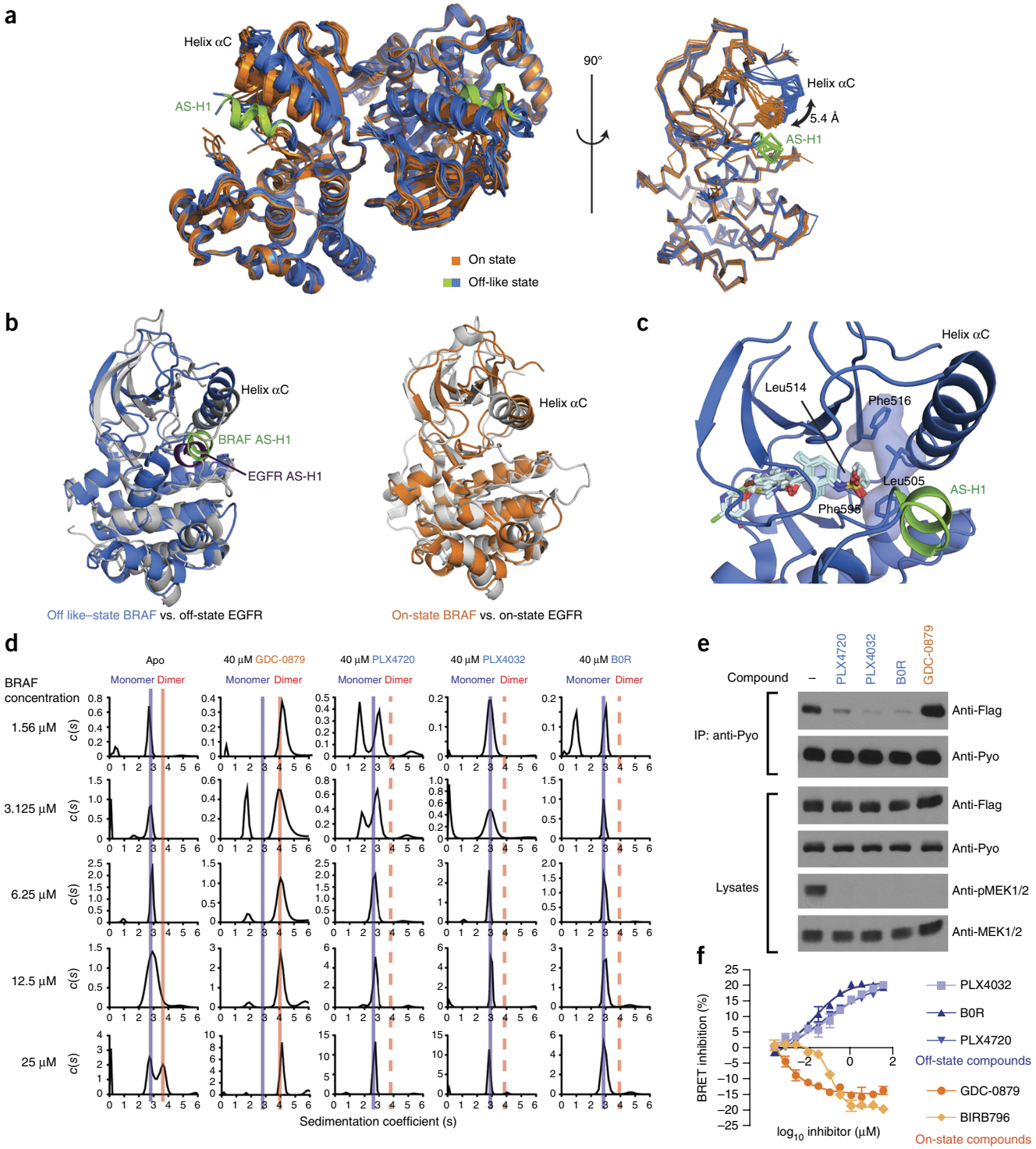

Figure 1 Inhibitors that induce an off state–like conformation of the BRAF kinase domain are dimer breakers in solution. (**a**) Superposition of ten on-state dimers (orange) and ten off state–like 'forced' dimers (blue). Right, frontal view of one kinase-domain protomer from each of the 20 structures, highlighting the lateral displacement of helix αC. Six of ten forced dimer structures display an on ordered helix AS-H1 (green) within the AS. (**b**) Comparison of on- and off-state BRAF dimer structures (PDB 1UWH[5] and PDB 3TV6 (ref. 29), respectively) with the on- and off-state structures of EGFR (PDB 2GS6 and PDB 2GS7 (ref. 12), respectively). (**c**) Binding mode of ten sulfonamide inhibitors to RAF, highlighting the engagement of a RAF-selective pocket (blue surface representation). (**d**) Sedimentation-velocity AUC analysis of the BRAF kinase domain in apo form or bound to GDC-0879, PLX4720, PLX4032 or B0R. Sedimentation-coefficient distribution (s) is plotted. (**e**) Co-IP of full-length Flag- and Pyo-tagged V600E BRAF and western blots of phosphorylated MEK (pMEK1/2) in serum-starved cells, treated for 1 h with DMSO or 10 μM of PLX4720, PLX4032, B0R or GDC-0879. Uncropped versions of western blots are shown in **Supplementary Data Set 1**. (**f**) BRET analysis of V600E BRAF in the presence of PLX4720, PLX4032, B0R, GDC-0879 or BIRB796. The Hill coefficients for the dose-response curves produced with these compounds are 0.48, 0.42, 0.59, 0.86 and 1.36, respectively. Mean ± s.d. of three technical replicates. Results from one experiment (representative of three independent experiments) are shown.

These inhibitors share a common ATP-competitive binding mode to the BRAF kinase domain (**Fig. 1c**), with the R_2 moiety engaging the adenine-, ribose- and phosphate-binding pockets of the catalytic cleft and the core sulfonamide and the R_1 groups orienting toward helix αC, causing its lateral displacement from a prototypical on-state position.

The effect of sulfonamide engagement with the kinase active site on the position of helix αC arises from the occupancy of a 'RAF-selective' pocket by the alkyl- or aryl-1–sulfonamide moieties[15] (**Fig. 1c**). This selectivity pocket is lined by Leu505, Leu514, Phe516 and Phe595, and we reason that its occupancy forces helix αC into an outward position through steric hindrance between the R_1 moiety and the Leu505 side chain (**Fig. 1c**). The importance of this inhibitor binding mode for the helix 'αC-out' conformation is best visualized in the BRAF–PLX4720 and BRAF–PLX4032 co-structures (PDB 3C4C and 3OG7, respectively[15,16]), in which, notably, the RAF-selective pocket is occupied by inhibitor in only one protomer of each BRAF dimer, and only those protomers displayed the helix αC-out conformation. Either the second protomers of each BRAF dimer are free of sulfonamide inhibitor (PDB 3OG7, chain B[16]), or the sulfonamide inhibitor engages the kinase active site in an alternate binding mode that leaves the RAF-selective pocket unoccupied (PDB 3C4C, chain B[15]). Concomitantly, these second protomers display an on state–like position of helix αC (**Supplementary Fig. 1b**).

A second notable feature found in six of the ten sulfonamide co-structures is the presence of a short secondary-structure element, termed helix AS-H1, encompassing AS residues Leu597 to Trp604 and the phosphoregulatory sites Thr599 and Ser602 (**Supplementary Table 1**). In these structures, helix AS-H1 packs against helix αC in a manner previously observed only in off-state kinase-domain structures such as EGFR (**Fig. 1b**), ErbB3 and CDK2 (refs. 12–14,17) (**Supplementary Fig. 2a**), thus suggesting that helix AS-H1 has a role in maintaining an off-state conformation of BRAF.

A last indication that sulfonamide-bound structures are reflective of off state–like conformations of the BRAF kinase domain is the integrity of the regulatory (R) and catalytic (C) spines. In on-state kinase structures, conserved hydrophobic residues form two colinear columns of density that span the N- and C-terminal kinase lobes and that orient the lobes in a productive closed conformation for catalysis[18]. In the BRAF–sulfonamide co-structures, the C spine is properly formed, but the R spine, composed of Leu505, Phe516, Phe595 and His574, is slightly kinked, owing to a misposition (1.6 Å from colinearity with the other R-spine residues) of the Leu505 side chain arising from the outward position of helix αC (**Supplementary Fig. 2a**). In contrast, all other BRAF dimer structures engaging type I or type II inhibitors clearly display intact and colinear C and R spines[19]. In the specific case of type II inhibitors, we previously noted that the substituted phenyl moieties of the bound inhibitors act as a surrogate to Phe595 in the R spine[19]. Although slightly distorted, the R spines of sulfonamide-bound structures are nonetheless continuous. This subtlety misled us to previously amalgamate the ten outlier dimer co-structures with other BRAF dimer co-structures in which the bound inhibitors were proven or inferred to promote dimerization[19].

Given that helix αC and the flanking loop contribute substantially to the side-to-side dimer interface (434.8 Å^2 of the 1,171.4 Å^2) and also contribute residues to the kinase active site, including Leu505 of the RAF-selective inhibitor–binding pocket[15], we hypothesized that helix αC could provide a conduit to allosterically link the two functionally important regions. Furthermore, we questioned whether sulfonamide inhibitors actually promoted dimerization, as inferred from crystal packing, or instead compromised the dimerization ability of the BRAF kinase domain relative to inhibitors that correlated with productive positions of helix αC. To test this hypothesis, we performed analytical ultracentrifugation (AUC) analysis on the isolated kinase domain of BRAF in the presence or absence of a representative set of inhibitors. As reported previously[19], apo wild-type (WT) BRAF kinase domain demonstrated a weak propensity to dimerize at high protein concentrations (**Fig. 1d**). In the presence of the kinase inhibitor GDC-0879 (which correlates with an inward active–like position of helix αC in its co-structures), WT BRAF was exclusively dimeric at all protein concentrations tested. Strikingly, however, WT BRAF in the presence of saturating concentrations (40 μM) of the sulfonamide inhibitors PLX4720, PLX4032 and B0R was exclusively monomeric at all protein concentrations tested (**Fig. 1d**). Analyses at lower inhibitor concentrations (2.5 and 10 μM) revealed that PLX4032 and B0R were more potent at inhibiting dimerization than PLX4720 (**Supplementary Fig. 1c**).

Next, we verified that the ability of sulfonamides to impede BRAF kinase domain homodimerization *in vitro* extends to a cell setting with full-length BRAF. In cells, RAF dimerization is dependent on Ras activity[20,21]. To avoid potential confounding effects of Ras on our experimental system, we took advantage of the behavior of full-length V600E BRAF, which forms dimers independently of Ras stimulation[22,23]. As assessed by coimmunoprecipitation (co-IP) (**Fig. 1e**), the kinase inhibitor GDC-0879 enhanced dimerization of V600E BRAF (**Fig. 1e**; lane 5). In contrast, dimerization was strongly reduced in the presence of PLX4720, PLX4032 and B0R (**Fig. 1e**; lanes 2–4). In agreement with these co-IP results, GDC-0879 and BIRB796, a second inhibitor whose co-structure with BRAF correlated with a productive position of helix αC[19], promoted BRAF dimerization of V600E BRAF in cells, as assessed by an increase in bioluminescence resonance energy transfer (BRET) signal, whereas PLX4720, PLX4032 and B0R reduced the BRET signal (**Fig. 1f**).

Together, these results indicate that despite cocrystallizing with the BRAF kinase domain in the side-to-side dimer configuration corresponding to a presumptive on-state conformation, the sulfonamide compounds are, in fact, BRAF homodimer breakers *in vitro* and in cells. We reason that the high concentration of BRAF proteins used in crystallization experiments forced a dimer configuration in the crystal environment that was not intrinsically favored by the BRAF–sulfonamide complexes *in vitro* and in cells.

Crystal structure of a BRAF monomer

Our observation that the examined sulfonamide inhibitors are breakers of BRAF dimers both *in vitro* and in cells led us to search for alternate conditions for cocrystallization of inhibitors with the BRAF kinase domain, in the hope of sampling the BRAF monomer state. In testing combinations of three different sulfonamides with WT BRAF kinase domain or the side-to-side dimer-interface mutant R509H, we found that PLX4720 cocrystallized with the WT BRAF kinase domain (**Fig. 2a** and **Table 1**) in a new packing arrangement not observed previously. The asymmetric unit of this new crystal form contains two BRAF molecules each in a monomeric configuration. None of the crystal contacts made by the BRAF monomer were large enough in surface area to suggest functional relevance in solution, and moreover none were conserved across the two molecules in the asymmetric unit (**Supplementary Fig. 3**).

The binding mode of PLX4720 in the monomer BRAF crystal structure is highly similar to that determined for PLX4720 and other sulfonamides bound in dimer BRAF crystal structures (**Fig. 1c**

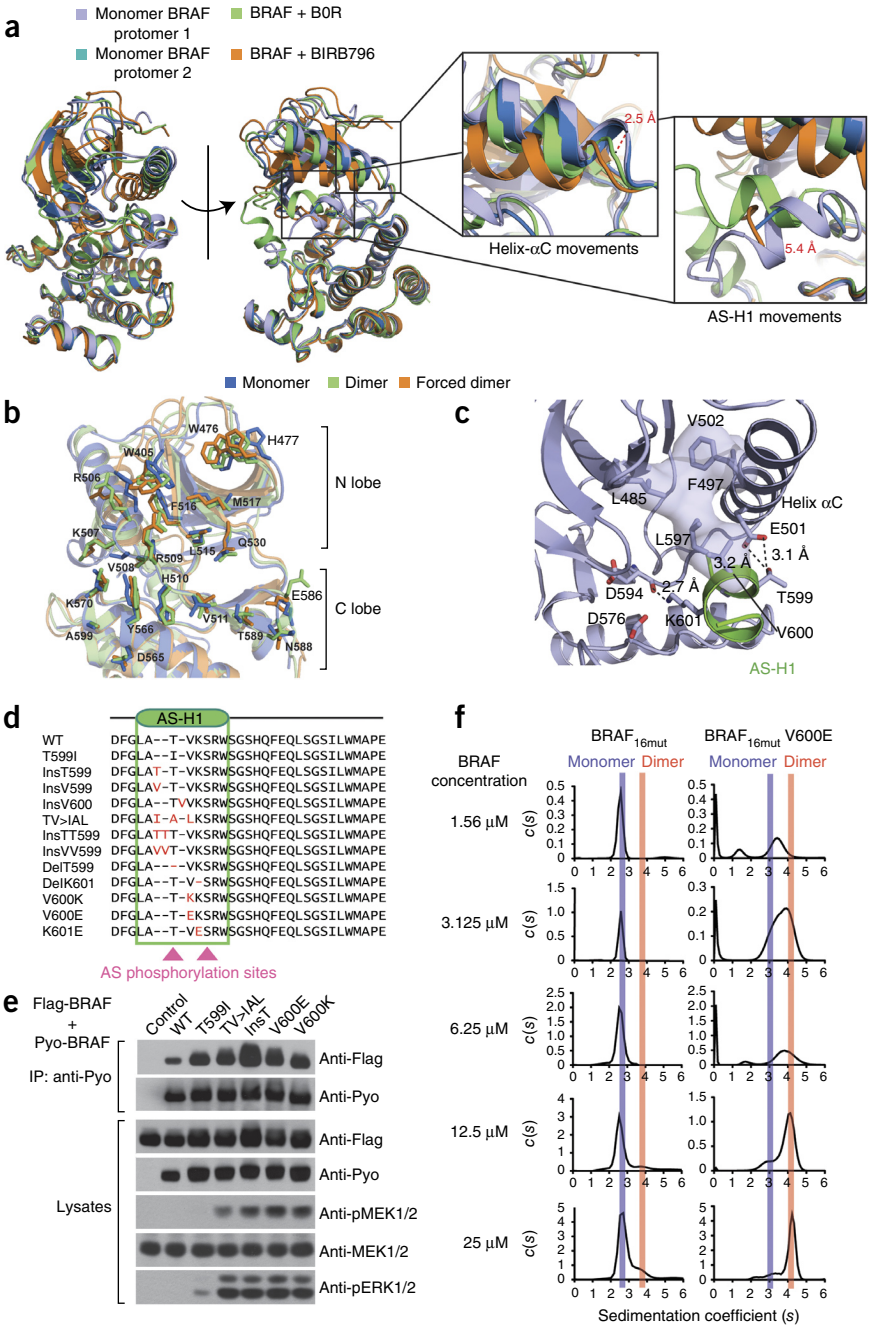

Figure 2 Crystal structure of a BRAF monomer yields insights in the allosteric control by dimerization by the AS. (**a**) Comparison of monomeric off-state BRAF (blue and light blue) with dimeric on-state RAF bound to BIRB796 (orange) and intermediate forced dimer states bound to B0R (green). Insets show close ups of the C-terminal end of helix αC (right) and helix AS-H1 (left). (**b**) Comparison of the side-to-side dimer-interface residues between monomeric BRAF, on-state dimers of BRAF (PDB 4JVG[19]) and forced dimers of BRAF (PDB 3TV6 (ref. 29)). (**c**) Interactions within the kinase active site of monomeric BRAF that stabilize an outwardly rotated helix αC and position helix AS-H1. (**d**) Sequence alignment of the BRAF AS, highlighting oncogenic mutations (red lettering). (**e**) BRAF co-IP and pMEK1/2, Flag and Pyo western blots from serum-starved cells expressing full-length BRAF WT or the AS-H1 mutants T599I, TV>IAL, InsT, V600E or V600K. Uncropped versions of western blots are shown in **Supplementary Data Set 1**. (**f**) Sedimentation-velocity AUC analysis of the oligomerization of BRAF kinase domain WT and V600E. Both these proteins comprised 16 solubilizing mutations ($BRAF_{16mut}$).

and **Supplementary Fig. 2b**). In addition, the kinase domains of the BRAF monomers appear more similar overall to the outlier sulfonamide-bound BRAF dimer structures, with all displaying an outwardly shifted helix αC, presence of helix AS-H1 and a kinked R spine (**Fig. 2a** and **Supplementary Fig. 2a**). However, in the monomer BRAF structures displacement of helix αC is much more exaggerated. Specifically, with the Cα position of residue Lys507 as a reference, the C-terminal end of helix αC is further shifted 2.5 Å outward in the monomer compared to dimer sulfonamide co-structures (**Fig. 2a**). This shift in helix αC correlates with a shift in the position of helix AS-H1 (an average of ~4.3 Å; **Fig. 2a**) and a further 0.6-Å outward shift in the position of Leu505. The latter increases the degree of kink in the regulatory spine so that it more closely approaches that of the completely broken spine conformation observed in the off-state structure of CDK enzymes (**Supplementary Fig. 2a**).

The exaggerated shift of helix αC in the monomer structures correlates with a change in position of the side chains on the side-to-side dimerization surface (**Fig. 2b**). We note that in all side-to-side dimer structures (i.e., both sulfonamide and other co-structures) these same side chains adopt highly similar positions (**Supplementary Fig. 2c**). Notably, among those, the side chains of Arg509 and Lys507 are ordered in all dimeric co-structures, whereas they appear highly mobile in monomeric BRAF. We reason that the positional change to dimer-interface residues is directly responsible for the reduced dimerization potential of RAF kinase domains when bound to sulfonamides *in vitro* and in cells. We also reason that the monomer state is the preferred structure of the kinase domain in solution when bound to sulfonamides and that forcing the kinase domain to concurrently crystallize in a dimer configuration while bound to a sulfonamide gave rise to an intermediate-hybrid conformation reminiscent of both true monomer and dimer states.

Helix AS-H1 and its role in BRAF oncogenic activation

In addition to inhibitor-specific interactions, notable interactions between kinase-domain elements, including between helix αC, helix AS-H1 and the surrounding active site, appear to support the outwardly displaced conformation of helix αC in the BRAF monomer. Phe497 on helix αC, Leu485 on strand β3, Leu597 on the AS and Val600 on helix AS-H1 together form a tightly packed hydrophobic network (**Fig. 2c**) contiguous with the hydrophobic RAF-selective pocket exploited for sulfonamide binding (**Fig. 1c**). In addition, Leu597 and Val600 sterically inhibit formation of the essential salt-bridge interaction between Glu501 (subdomain III residue on αC) and Lys483 (subdomain II reside on β3) that defines the on state

Table 1 Data collection and refinement statistics

	Monomeric BRAF
Data collection	
Space group	*I*222
Cell dimensions	
a, *b*, *c* (Å)	65.61, 72.75, 243.34
Resolution (Å)	38.03–2.83 (2.99–2.83)[a]
R_{sym}	0.072 (0.48)
$I / \sigma I$	20.2 (3.6)
Completeness (%)	99.9 (100.0)
Redundancy	6.5 (6.8)
Refinement	
Resolution (Å)	2.83
No. reflections	93,783 (total) / 14,335 (unique)
R_{work} / R_{free}	19.3 / 26.1
No. atoms	
Protein	3,978
Ligand/ion	54
Water	77
B-factors	
Protein	57.76
Ligand/ion	41.91
Water	49.64
r.m.s. deviations	
Bond lengths (Å)	0.009
Bond angles (°)	1.19

[a]Values in parentheses are for highest-resolution shell. Each structure was solved by molecular replacement with data from a single crystal.

of prototypical protein kinases (**Fig. 2c**). Glu501 instead engages in a hydrogen-bond interaction with Thr599 (one of two proven AS phosphoregulatory sites) within helix AS-H1, while Lys601 in helix AS-H1 hydrogen-bonds to the main chain carbonyl of Asp594 as well as to the main chain carbonyl of His574 and the side chain of Asp576 of the HRD motif (**Fig. 2c**). As noted above, a similarly configured helix AS-H1 is apparent in the off-state structure of the EGFR kinase domain (**Fig. 1b**), and the predicted structure-disrupting mutation L858R within helix AS-H1 of EGFR has been shown to cause oncogenic activation[12] and dimerization[24]. This led us to hypothesize that helix AS-H1 has a similarly important role in the maintenance of the off state of RAF in the absence of sulfonamide binding. If true, then this model would provide a more precise basis to explain the mechanism by which oncogenic mutations within the AS of BRAF might act.

Strikingly, the most frequent BRAF oncogenic mutations, including the prevalent V600E and V600K substitutions as well as less frequent insertions and deletions, are located in helix AS-H1 (**Fig. 2d**). All of these mutations are predicted to perturb the structure of helix AS-H1 and, in turn, destabilize the outward position of helix αC. Because the position of helix αC provides a link to the dimerization infrastructure, we reason that the oncogenic BRAF mutations within helix AS-H1 also promote the dimerization of full-length BRAF in cells, as assessed by co-IP, and the dimerization of the isolated kinase domain, as assessed by AUC. As predicted, dimerization of all oncogenic helix AS-H1 mutants tested, including T599I, TV>IAL, insT, V600K and V600E, was sharply increased compared to that of the WT protein in co-IP experiments (**Fig. 2e**). Similarly, the prevalent V600E mutant displayed increased dimerization potential relative to that of WT protein, as assessed by AUC (**Fig. 2e**,**f**).

From comparative modeling to AKT, Wan *et al.* predicted that the V600E substitution generates a salt bridge between the side chains of Glu600 and Lys507 (located at the C-terminal end of helix αC) that may stabilize productive conformations of both the AS and αC helix[5]. In support for this hypothesis, the crystal structure of a V600E BRAF mutant allowed direct visualization of the predicted interaction (PDB 3OG7, unoccupied protomer[16]) (**Fig. 3a**). To test whether the Glu600-Lys507 salt interaction contributed to the enhanced catalytic function of the V600E mutant, we substituted Lys507 with glutamate in combination with different charge mutations at Val600. We evaluated the full-length mutant proteins for downstream signaling, by assessing pMEK1 and pMEK2 levels (**Fig. 3b**), as well as for dimerization, by co-IP (**Fig. 3c**). In agreement with the Glu600-Lys507 salt-bridge model, the K507E V600E double mutant exhibited considerably reduced activity and dimerization potential (**Fig. 3b**,**c**; lanes 3 and 4). In sharp contrast, the V600K K507E double mutant displayed increased activity and enhanced dimerization (**Fig. 3b**,**c**; lanes 6 and 7). Therefore, these findings provide experimental evidence supporting the notion of a functional salt bridge between Glu600 and K507 and may explain in part the high prevalence and the strong kinase activity of this particular BRAF mutation.

In agreement with three previous reports[4,22,23], and in contrast to that of WT BRAF, the activity of the V600E allele expressed in mammalian cells was not affected by the mutation of a key side-to-side interface residue (R509H) that severely disrupts dimerization (**Fig. 3b**,**c**; lanes 3 and 5). We made the same observation for the V600K allele (**Fig. 3b**,**c**; lanes 6 and 8). Together, these results suggest that in cells the Val600 mutations enable the kinase domain to reach a sufficiently active state independently of dimerization. Therefore, the ability of the K507E mutation to impede dimerization of the V600E variant probably does not fully account for the reduced activity of the K507E V600E double mutant. Instead, the loss of activity is likely to reflect, in part, the repulsive interaction between the two glutamate residues that disfavors the attainment of a productive conformation of the AS.

We observed a similar trend when measuring the *in vitro* catalytic function of a similar panel of bacterially expressed and purified BRAF mutant kinase domains, results in agreement with our in-cell findings. Interestingly, the K507E mutation alone lowered catalytic activity relative to that of the WT enzyme (**Fig. 3d**; lanes 2 versus 3), thus demonstrating that this residue is functionally important when no oncogenic mutations are present in helix AS-H1. In the WT Lys507 background, the V600E mutant was much more potent than the V600K mutant in phosphorylating MEK1 (**Fig. 3d**; lanes 4 versus 6) and, similarly to observations in cells, the K507E mutation dramatically reduced the activity of the V600E mutant, whereas it enhanced the activity of the V600K mutant (**Fig. 3d**; comparison of lanes 5 and 7). However, unlike the situation in cells, the activity of the bacterially expressed V600E BRAF kinase domain was sensitive to the R509H mutation (**Fig. 3e**). This observation suggests that other factors may contribute to the dimerization-independent function of the V600E oncogenic mutation, possibly including known regulators of RAF activation, such as Ras and 14-3-3, and post-translational modifications that were absent from the *in vitro* analysis. Finally, we were unable to perform follow-on AUC studies on isolated kinase domains bearing the K507E mutation to complement our co-IP results, owing to reductions in protein solubility. Overall, however, our results are consistent with the notion that, in addition to destabilizing the off-state conformation of helix AS-H1, Glu600 also forms a favorable salt interaction with Lys507 that stabilizes the on-state conformation of the AS, thus conferring enhanced signaling potency to the V600E oncogenic mutant.

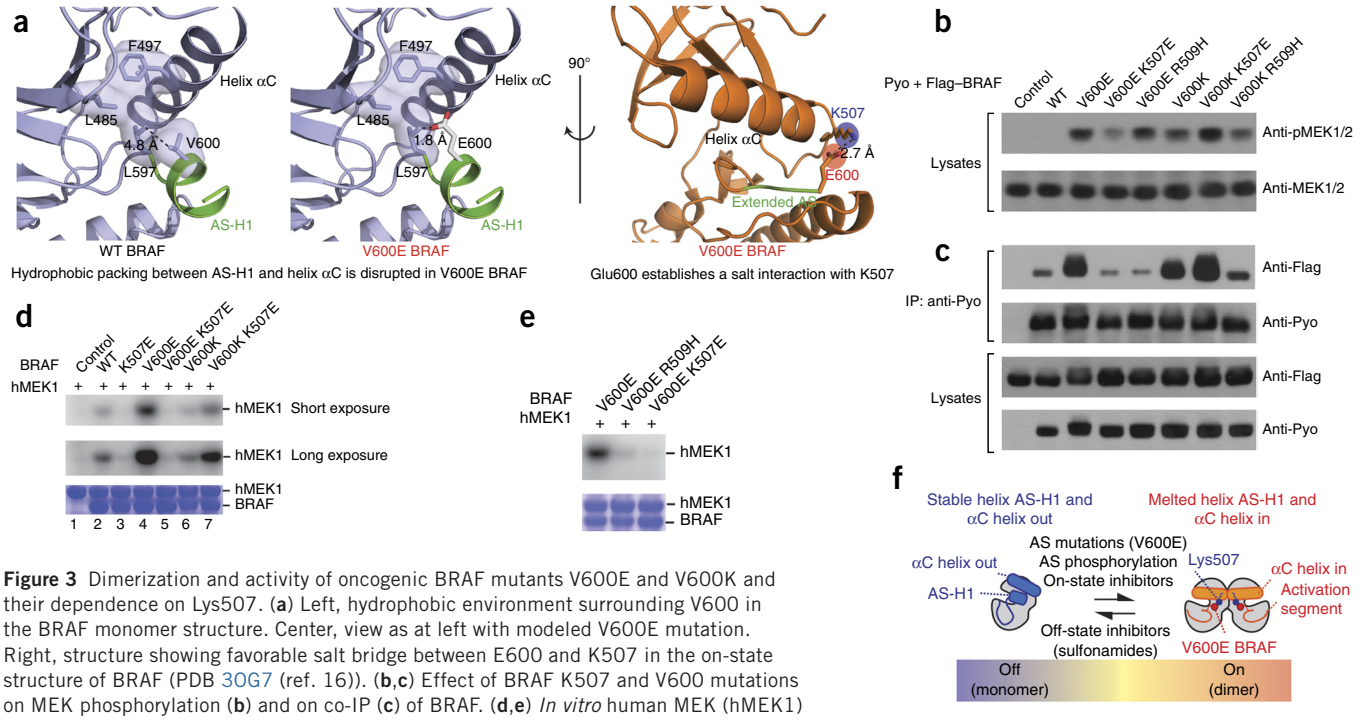

Figure 3 Dimerization and activity of oncogenic BRAF mutants V600E and V600K and their dependence on Lys507. (**a**) Left, hydrophobic environment surrounding V600 in the BRAF monomer structure. Center, view as at left with modeled V600E mutation. Right, structure showing favorable salt bridge between E600 and K507 in the on-state structure of BRAF (PDB 3OG7 (ref. 16)). (**b**,**c**) Effect of BRAF K507 and V600 mutations on MEK phosphorylation (**b**) and on co-IP (**c**) of BRAF. (**d**,**e**) *In vitro* human MEK (hMEK1) phosphorylation assays with WT and mutants of the BRAF kinase domain. Uncropped versions of images in **b**–**e** are shown in **Supplementary Data Set 1**. (**f**) Model depicting the allosteric regulation of BRAF off-on switching by conformations of the AS and the αC helix.

DISCUSSION

The previous and newly determined co-structures with sulfonamide inhibitors provide new insight into the nature of the BRAF monomer off state, complementing the more developed understanding of the BRAF dimer on state. With these structural reference points as guides, we can now infer how self-association through the side-to-side dimer interface, together with AS phosphorylation, allosterically regulates protein kinase catalytic function under normal, disease-state and drug-modulated conditions (regulatory model in **Fig. 3f**). The off-state monomer configuration of the BRAF kinase domain (**Fig. 3f**) is incompetent for phosphotransfer because helix αC is displaced from a productive orientation, thereby disrupting the integrity of the R spine and precluding formation of the essential Lys483-Glu501 salt bridge required to coordinate the ATP phosphate groups. Helix AS-H1 within a dephosphorylated AS actively supports the nonproductive position of helix αC, which in turn disfavors attainment of the side-to-side dimer configuration. AS mutations that destabilize helix AS-H1 favor the attainment of a dimer-competent state associated with a productive inward orientation of helix αC (**Fig. 3f**). At this step of the activation process, a productive orientation of helix αC can reciprocally be imposed by side-to-side dimerization, thereby triggering the melting of helix AS-H1 and concomitant enhancement of enzyme phosphotransfer function. This 'αC-in' configuration with an extended AS is exemplified by BRAF co-structures with dimer-inducing kinase inhibitors (**Fig. 3f**)[19]. Finally, the V600E mutation can further promote the extended conformation of the AS through generation of positive salt-bridge interactions with Lys507 (**Fig. 3f**). This strengthens the αC-in conformation and, in turn, side-to-side dimerization and enzyme catalytic function. Because the regulatory sites Thr599 and Ser602 lie immediately adjacent to Val600, we speculate that the same principles may hold true during physiological activation of enzyme activity by phosphorylation of the AS. These regulatory features provide a basis to more precisely explain the mechanism of action of many cancer-causing mutations, which act through a combination of destabilization of nonproductive conformations and stabilization of productive conformations of the kinase AS. As appears to be the case for the V600E mutation, it is likely that some oncogenic mutations are sufficiently potent at stabilizing a productive conformation of helix αC and the AS in *cis* that the enzyme becomes relatively insensitive to the need for side-to-side dimerization despite displaying an enhanced ability to dimerize.

Intriguingly, the catalytic-switching model for RAF is highly reminiscent of that proposed for EGFR[12]. The off-state structures of both enzymes are defined by nonproductive positions of helix αC and the presence of a supporting short helical element in their ASs corresponding to helix AS-H1 in BRAF. Repositioning of helix αC to a productive orientation for catalysis is mediated in both cases by phosphorylation of regulatory sites in the AS and by self-association of the kinase domain. However, the precise modes of self-association underlying enzyme activation are drastically different. In the case of BRAF, self-association arises through a closed two-fold symmetric side-to-side arrangement of kinase domains, whereas for EGFR self-association arises from a head-to-tail arrangement of kinase domains that enables polymer formation. EGFR kinase domain function is modulated at a higher level by the binding of growth-factor ligands to the extracellular ligand-binding domain, which provides the main driving force for the self-association of kinase domains. Intramolecular interaction of the kinase domain with the juxtamembrane segment serves as a counter force to stabilize the resting monomeric state or an inactive dimer state[25,26]. In extension of these parallels to RAF, bivalent binding to 14-3-3 proteins serves as a powerful driver for the self-association of RAF kinase domains. Furthermore, regions N terminal to the kinase domain of RAF have been implicated in autoinhibition that is relieved, in part, by binding to RAS[27,28]. How the intramolecular modes interface with the dimerization and AS infrastructure of RAF to mediate this level of regulation remains to be structurally defined.

Finally, our findings provide insight into how the binding of small-molecule inhibitors to the kinase active site of BRAF can exert

differential effects on enzyme transactivation by either promoting or inhibiting side-to-side dimerization. The ability of inhibitors to bind the active site of one BRAF protomer and lead to the dimer-dependent transactivation of a second protomer is an unintended impediment to the generation of useful anticancer therapeutics. All dimer-promoting inhibitors exploit features of the enzyme on state defined by contiguous R and C spines[19]. Sulfonamides, however, are unique in exploiting features of the monomeric off state of BRAF. We note that our finding that sulfonamides can act as dimer breakers is so far limited to BRAF homodimers. Indeed, despite the ability of sulfonamides to induce an off-state conformation of the BRAF kinase domain, these molecules nevertheless induce BRAF–CRAF heterodimers in RAS-activated cells[6–8], although with lower potency than for other ATP-competitive RAF inhibitors[19]. The underlying cause of this differential effect on BRAF–BRAF homodimer and BRAF–CRAF heterodimer formation remains to be determined, but it may be due in part to intrinsic differences between homo- and heterodimer structures of the kinase domain or alternatively to extrinsic regulatory factors and events that impinge on full-length RAF dimerization. Further investigation is warranted. Last, although current sulfonamide inhibitors may be imperfect in preventing side-to-side dimerization in a crystal environment or, in the case of the different full-length RAF isoforms, in a physiological context in which RAS activity is elevated[6–8], they nonetheless provide insight into how better inhibitors may be engineered. We posit that next-generation inhibitors that bind to the kinase domain of BRAF in a fashion that distorts the position of helix αC and stabilizes the off-state conformation of the AS (specifically helix AS-H1) to totally preclude side-to-side dimerization will eliminate the detrimental transactivation phenomenon that limits the utility of some current drugs in the clinic.

METHODS

Methods and any associated references are available in the online version of the paper.

Accession codes. Coordinates and structure factors for monomeric $BRAF_{16mut}$ –PLX4720 have been deposited in the Protein Data Bank under accession code PDB 4WO5.

Note: Any Supplementary Information and Source Data files are available in the online version of the paper.

ACKNOWLEDGMENTS

We thank M. Gao from Bristol-Myers Squibb Molecular Structure & Design group for making BRAF expression constructs. N.T. is supported by an Ontario Graduate Scholarship and a Canadian Institutes for Health Research (CIHR) Canada Graduate Scholarship. H.L. is supported by a CIHR Banting Postdoctoral Fellowship. F.S. is supported as a Canada Research Chair. This work was supported by a grant from the Ministère de l'Économie, de l'Innovation et de l'Exportation du Québec to A.M. and an Impact Grant from the Canadian Cancer Society Research Institute to M.T. (702319) as well as by operating funds from the CIHR to M.T. (MOP119443) and F.S. (MOP36399).

AUTHOR CONTRIBUTIONS

N.T., H.L., F.S. and M.T. designed the experiments and wrote the manuscript. N.T. performed AUC experiments and *in vitro* kinase assays. H.L. performed BRET and co-IP experiments. D.A.C. conducted protein production, crystallization and X-ray data collection. Structural analysis of the BRAF monomer was performed by D.A.C., A.T., N.T. and H.L. A.M. provided expert advice for the interpretation of compound binding mode.

COMPETING FINANCIAL INTERESTS

The authors declare no competing financial interests.

1. Rajakulendran, T., Sahmi, M., Lefrancois, M., Sicheri, F. & Therrien, M. A dimerization-dependent mechanism drives RAF catalytic activation. *Nature* **461**, 542–545 (2009).
2. Zhang, B.H. & Guan, K.L. Activation of B-Raf kinase requires phosphorylation of the conserved residues Thr598 and Ser601. *EMBO J.* **19**, 5429–5439 (2000).
3. Chong, H., Lee, J. & Guan, K.L. Positive and negative regulation of Raf kinase activity and function by phosphorylation. *EMBO J.* **20**, 3716–3727 (2001).
4. Freeman, A.K., Ritt, D.A. & Morrison, D.K. Effects of Raf dimerization and its inhibition on normal and disease-associated Raf signaling. *Mol. Cell* **49**, 751–758 (2013).
5. Wan, P.T. *et al.* Mechanism of activation of the RAF-ERK signaling pathway by oncogenic mutations of B-RAF. *Cell* **116**, 855–867 (2004).
6. Heidorn, S.J. *et al.* Kinase-dead BRAF and oncogenic RAS cooperate to drive tumor progression through CRAF. *Cell* **140**, 209–221 (2010).
7. Poulikakos, P.I., Zhang, C., Bollag, G., Shokat, K.M. & Rosen, N. RAF inhibitors transactivate RAF dimers and ERK signalling in cells with wild-type BRAF. *Nature* **464**, 427–430 (2010).
8. Hatzivassiliou, G. *et al.* RAF inhibitors prime wild-type RAF to activate the MAPK pathway and enhance growth. *Nature* **464**, 431–435 (2010).
9. Garnett, M.J. & Marais, R. Guilty as charged: B-RAF is a human oncogene. *Cancer Cell* **6**, 313–319 (2004).
10. Kandoth, C. *et al.* Mutational landscape and significance across 12 major cancer types. *Nature* **502**, 333–339 (2013).
11. Forbes, S.A. *et al.* COSMIC: mining complete cancer genomes in the Catalogue of Somatic Mutations in Cancer. *Nucleic Acids Res.* **39**, D945–D950 (2011).
12. Zhang, X., Gureasko, J., Shen, K., Cole, P.A. & Kuriyan, J. An allosteric mechanism for activation of the kinase domain of epidermal growth factor receptor. *Cell* **125**, 1137–1149 (2006).
13. Shi, F., Telesco, S.E., Liu, Y., Radhakrishnan, R. & Lemmon, M.A. ErbB3/HER3 intracellular domain is competent to bind ATP and catalyze autophosphorylation. *Proc. Natl. Acad. Sci. USA* **107**, 7692–7697 (2010).
14. Jeffrey, P.D. *et al.* Mechanism of CDK activation revealed by the structure of a cyclinA-CDK2 complex. *Nature* **376**, 313–320 (1995).
15. Tsai, J. *et al.* Discovery of a selective inhibitor of oncogenic B-Raf kinase with potent antimelanoma activity. *Proc. Natl. Acad. Sci. USA* **105**, 3041–3046 (2008).
16. Bollag, G. *et al.* Clinical efficacy of a RAF inhibitor needs broad target blockade in BRAF-mutant melanoma. *Nature* **467**, 596–599 (2010).
17. De Bondt, H.L. *et al.* Crystal structure of cyclin-dependent kinase 2. *Nature* **363**, 595–602 (1993).
18. Kornev, A.P., Haste, N.M., Taylor, S.S. & Eyck, L.F. Surface comparison of active and inactive protein kinases identifies a conserved activation mechanism. *Proc. Natl. Acad. Sci. USA* **103**, 17783–17788 (2006).
19. Lavoie, H. *et al.* Inhibitors that stabilize a closed RAF kinase domain conformation induce dimerization. *Nat. Chem. Biol.* **9**, 428–436 (2013).
20. Luo, Z. *et al.* Oligomerization activates c-Raf-1 through a Ras-dependent mechanism. *Nature* **383**, 181–185 (1996).
21. Weber, C.K., Slupsky, J.R., Kalmes, H.A. & Rapp, U.R. Active Ras induces heterodimerization of cRaf and BRaf. *Cancer Res.* **61**, 3595–3598 (2001).
22. Röring, M. *et al.* Distinct requirement for an intact dimer interface in wild-type, V600E and kinase-dead B-Raf signalling. *EMBO J.* **31**, 2629–2647 (2012).
23. Poulikakos, P.I. *et al.* RAF inhibitor resistance is mediated by dimerization of aberrantly spliced BRAF(V600E). *Nature* **480**, 387–390 (2011).
24. Shan, Y. *et al.* Oncogenic mutations counteract intrinsic disorder in the EGFR kinase and promote receptor dimerization. *Cell* **149**, 860–870 (2012).
25. Arkhipov, A. *et al.* Architecture and membrane interactions of the EGF receptor. *Cell* **152**, 557–569 (2013).
26. Endres, N.F. *et al.* Conformational coupling across the plasma membrane in activation of the EGF receptor. *Cell* **152**, 543–556 (2013).
27. Tran, N.H., Wu, X. & Frost, J.A. B-Raf and Raf-1 are regulated by distinct autoregulatory mechanisms. *J. Biol. Chem.* **280**, 16244–16253 (2005).
28. Chong, H. & Guan, K.L. Regulation of Raf through phosphorylation and N terminus-C terminus interaction. *J. Biol. Chem.* **278**, 36269–36276 (2003).
29. Wenglowsky, S. *et al.* Pyrazolopyridine inhibitors of B-Raf(V600E). Part 1: the development of selective, orally bioavailable, and efficacious inhibitors. *ACS Med. Chem. Lett.* **2**, 342–347 (2011).

ONLINE METHODS

Plasmids. $BRAF_{444–72}$ (ref. 3), used in AUC analysis, was cloned with 16 solubilizing mutations[1] (I543A, I544S, I551K, Q562R, L588N, K630S, F667E, Y673S, A688R, L706S, Q709R, S713E, L716E, S720E, P722S, and K723G), referred to as $BRAF_{16mut}$, into pPROEX-HTa (Invitrogen) between NcoI and NotI sites. For co-IP experiments, either a Pyo tag or a Flag tag was added at the N terminus of the full-length BRAF cDNA by PCR and was cloned between KpnI and XbaI in a pCDNA3.1-Hygro plasmid. All mutants were generated by PCR-based site-directed mutagenesis with standard procedures. Human $MEK1_{37–393}$ (hMEK1) used in *in vitro* kinase assays was cloned with a C-terminal, noncleavable His_6 tag into pProEX-HTA between engineered NcoI and XbaI sites, which replaced the N-terminal His_6 tag and TEV-cleavage site. A second construct of $BRAF_{444–723}$ containing the aforementioned 16 solubilizing mutations[15] and which was used for PLX4720 cocrystallography was cloned into a pET28 expression vector with an N-terminal TVMV protease–cleavable His_6 tag.

Protein purification. WT BRAF and $BRAF_{16mut}$ with TEV-cleavable His_6 tags were expressed in BL21(DE3)-RIL bacterial expression cells, purified with nickel-affinity chromatography, TEV-cleaved overnight and purified through gel-filtration chromatography into a final buffer of 15 mM HEPES, pH 7.5, 200 mM NaCl, 10 mM DTT, and 5% (v/v) glycerol. After gel filtration, protein fractions corresponding to greater than 95% purity were pooled and concentrated to 20 mg/mL, then flash frozen in liquid nitrogen. $BRAF_{16mut}$ with a TVMV protease–cleavable His_6 tag was expressed in Rosetta 2 BL21 bacterial expression cells and purified by sequential nickel-affinity and gel-filtration chromatographies into a final buffer of 20 mM HEPES, pH 7.5, 200 mM NaCl, 1 mM TCEP, and 5% (v/v) glycerol. After gel filtration, protein fractions corresponding to greater than 95% purity were pooled and concentrated to ~19 mg/mL, after which cocrystallization screening was immediately carried out.

Analytical ultracentrifugation (AUC). Sedimentation-velocity AUC was performed with a Beckman ProteomeLab XL-I at 42,000 r.p.m. Data were obtained after 7.5 h of centrifugation at 20 °C by monitoring the relative refractive index between sample and blank. Various concentrations of $BRAF_{16mut}$, ranging from 1.56 μM to 25 μM, were tested minimally in duplicate in AUC buffer (for AUC with compound, 15 mM HEPES, pH 7, 200 mM NaCl, and 3 mM DTT; for AUC of $BRAF_{16mut}$ mutants, 15 mM HEPES, pH 7, 250 mM NaCl, 10 mM DTT, and 5% glycerol) in the presence or absence of 2.5 μM, 10 μM or 40 μM inhibitor compound.

***In vitro* kinase assay.** 8 μM $BRAF_{16mut}$ mutants were incubated with 10 μM hMEK1 in 15 mM HEPES, 5% glycerol, 2 mM $MgCl_2$, 200 mM NaCl and 10 mM DTT. Reactions were started with the addition of 120 μM ATP (4:1 ATP to [γ-^{32}P]ATP) and were conducted for 30-min and 1-h intervals.

Protein crystallization, data collection and structural analysis. 266 μM (9.1 mg/mL) $BRAF_{16mut}$ was cocrystallized with 816 μM PLX4720 at 22 °C in 0.1 M trimethylamine-*N*-oxide, 50 mM Tris, pH 8.5, and 10% (w/v) PEG monomethylether with the sitting-drop vapor-diffusion method. X-ray diffraction data were collected on a flash-frozen crystal cryoprotected in mother liquor containing 25% glycerol at a wavelength of 1.0 Å and temperature of 100 K at the Advanced Photon Source (IMCA-CAT beamline 17-ID). Data reduction was performed with autoPROC[30]. The $BRAF_{16mut}$–PLX4720 co-structure was solved by molecular replacement with PDB 3C4C[15] as a search model in Phaser[31]. Model building and refinement were performed with Coot[32] and autoBUSTER (Global Phasing Ltd.), respectively.

Inhibitors used in this study. PLX4720, PLX4032 and GDC-0879 were obtained from Selleck chemicals. B0R was synthesized by Union Biopharma. All compounds were at least 95% pure, as evaluated by HPLC. All were prepared as stock solutions in DMSO at 100 mM. For BRET dose-response experiments, serial dilutions of drugs were prepared in DMSO, and 1:100 dilutions were prepared in Tyrode's buffer before addition to 90 μl of cell suspensions in Tyrode's buffer (1×10^6 cells/ml) at a 1:10 dilution for the indicated time.

Cell culture, transfection and BRET assays. HEK293T cells were maintained in DMEM supplemented with 10% FBS. Cells were routinely tested for mycoplasma contamination. For co-IP experiments, 2.5×10^6 cells were transfected with Pyo- and Flag-tagged BRAF constructs with PEI. Cells were serum starved by incubation overnight in DMEM without FBS after being washed twice in 1× PBS. BRET dose-response experiments were conducted as previously described[19]. BRET signals and luciferase activity were read 15 min after addition of 2.5 μM Coelenterazine 400a (Biotium) with a Mithras LB940 plate reader (Berthold Technologies) equipped with BRET2 emission filter set (donor, 410 nm ± 70 nm; acceptor, 515 nm ± 20 nm). BRET signals correspond to the light emitted by the GFP10 acceptor constructs (515 nm ± 20 nm) upon addition of Coelenterazine 400a divided by the light emitted by the RlucII donor constructs (410 nm ± 70 nm). Compound influence on the BRET probes was expressed as a percentage of BRET inhibition, calculated as follows: $100 \times (1 - (BRET_{compound}/BRET_{DMSO}))$.

Coimmunoprecipitation and western blotting. Coimmunoprecipitation and western blotting procedures were essentially conducted as follows. To prepare cell lysates, cells were washed once in cold 1× PBS and then directly lysed on plates by addition of 1 ml of Igepal lysis buffer (20 mM Tris, pH 8.0, 137 mM NaCl, 10% glycerol, 1% Igepal CA-630, 2 mM EDTA, 1× phosphatase-inhibitor cocktail (Sigma), 1 mM sodium vanadate, 20 μM leupeptin and aprotinin (0.15 U/ml), and 1 mM PMSF). Lysing cells were incubated for 10 min at 4 °C with gentle rocking, collected and spun at 14,000*g* at 4 °C for 10 min. For coimmunoprecipitations, 100 μl of anti-Pyo primary antibody was added to fresh cell lysates and incubated at 4 °C for 2 h. Protein A/G agarose beads (Santa Cruz Biotechnology) were then added and gently rocked at 4 °C for an additional 2 h. Immunoprecipitates were washed four times with cold lysis buffer. Anti-Pyo IPs and cell lysates were boiled in sample buffer for 5 min. IPs and cell lysates were then resolved on 10% SDS-PAGE, transferred to nitrocellulose membranes (Dupont) and probed with appropriate primary antibodies. All antibodies were diluted in Tris-buffered saline (TBS) supplemented with 0.2% Tween. Anti–phospho MEK (Cell Signaling Technology; cat. no. 9121) and anti-MEK1/2 (Cell Signaling Technology; cat. no. 9122) were used at 1:2,000 dilution. Anti-Flag M2 (Sigma; cat. no. F1804) was used at 1:5,000 dilution. Validation information is provided on the manufacturers' websites for all commercially available antibodies used in this work. Anti-Pyo supernatants are routinely validated on transfected HEK293T cells. Anti-Pyo supernatant from hybridoma[33,34] was used at 1:10 dilution. Secondary anti-mouse and anti-rabbit HRP (Jackson Immunoresearch; cat. nos. 115-035-146 and 111-035-144, respectively) were used at 1:10,000 dilution in TBS-0.2% Tween.

Data analysis and structure rendering. All protein structure representations were prepared with PyMOL (http://www.pymol.org/). AUC data were processed with SEDFIT (http://www.analyticalultracentrifugation.com/default.htm) to calculate a continuous c(s) distribution. Solute partial specific volume, buffer density and buffer viscosity were calculated with Sednterp (http://sednterp.unh.edu/). BRET data were analyzed with Prism 5.04 (GraphPad Software). EC_{50} values were calculated with a log(agonist) versus response fitting.

30. Vonrhein, C. *et al.* Data processing and analysis with the autoPROC toolbox. *Acta Crystallogr. D Biol. Crystallogr.* **67**, 293–302 (2011).
31. Adams, P.D. *et al.* PHENIX: a comprehensive Python-based system for macromolecular structure solution. *Acta Crystallogr. D Biol. Crystallogr.* **66**, 213–221 (2010).
32. Emsley, P., Lohkamp, B., Scott, W.G. & Cowtan, K. Features and development of Coot. *Acta Crystallogr. D Biol. Crystallogr.* **66**, 486–501 (2010).
33. Douziech, M. *et al.* Bimodal regulation of RAF by CNK in *Drosophila*. *EMBO J.* **22**, 5068–5078 (2003).
34. McKay, M.M. & Morrison, D.K. Proteomic analysis of scaffold proteins in the ERK cascade. *Methods Mol. Biol.* **661**, 323–334 (2010).

doi:10.1038/nsmb.2924